Effects of Molecular Weight on the Structure of Poly(phenylene sulfide) Crystallized at Low Temperatures

ARTICLE *in* MACROMOLECULES · OCTOBER 1997

Impact Factor: 5.8 · DOI: 10.1021/ma961600e

Effects of Molecular Weight on the Structure of Poly(phenylene sulfide) Crystallized at Low Temperatures

Sharon Xin Lu[†] and Peggy Cebe*

Department of Physics and Astronomy, Science and Technology Center, Tufts University, Medford, Massachusetts 02155

Malcolm Capel

Biology Department, Brookhaven National Laboratory, Upton, New York, 11973

Received October 29, 1996; Revised Manuscript Received August 2, 1997[⊗]

ABSTRACT: We report a study of the effects of molecular weight on the structure and properties of poly(phenylene sulfide), PPS, crystallized from the rubbery amorphous state at temperatures just above the glass transition. PPS films were characterized using temperature-modulated differential scanning calorimetry (MDSC), small angle X-ray scattering (SAXS), and dynamic mechanical analysis (DMA). For samples crystallized so as to have the same half-time, we find (1) the degree of crystallinity, χ_c, is not dependent upon molecular weight and (2) as the molecular weight increases, the heat capacity increment at the glass transition increases. These results suggest that lower molecular weight PPS contains a greater fraction of the rigid amorphous phase, probably as a result of formation of taut tie molecules between crystals. It is found from DMA that molecular weight is the determining factor that affects the Young's modulus value at the higher temperature. A lower E' is observed for the higher molecular weight material. MDSC data suggest that higher molecular weight PPS has a slower crystallization rate and reorganization rate. The amount of crystals formed during heating is smaller in higher molecular weight PPS, and this may be the explanation for the reduced Young's modulus above T_g.

1. Introduction

Semicrystalline polymers may be regarded as composite materials comprising lamellar crystals separated by uncrystallized polymer. The highly entangled melt state is the usual starting point for crystallization studies in which the temperature of the melt is decreased to the crystallization temperature, T_c. As crystals grow in the entangled melt, chain constraints are created that limit the ultimate crystallinity that can be achieved and serve to constrain the molecular mobility of the uncrystallized amorphous material located in the "interlayer" between the crystals.

In some polymers with relatively stiffer chains and elevated glass transition temperatures (T_g), the crystallization rate is slower, and as the material is cooled rapidly through T_g, crystallization may be suppressed entirely. Examples of polymers that can be quenched to the glassy amorphous state are poly(ethylene terephthalate), PET, poly(ether ether ketone), PEEK, and poly(phenylene sulfide), PPS. When the quenched amorphous sample of these polymers is heated from below to above T_g, the molecular mobility increases and the previously amorphous chains may now crystallize. This affords the opportunity to study crystallization kinetics and structure development in these polymers at very low crystallization temperatures. In this work we examine the effects of molecular weight on the structure of PPS, which is crystallized very close to T_g.

Poly(phenylene sulfide) is an engineering thermoplastic polymer with a glass transition above room temperature (at 90°C) and a relatively low degree of crystallinity (<0.40) determined from differential scanning calorimetry (DSC).[1−7] PPS can be crystallized either from the melt or from the rubbery amorphous state. Crystallinity, glass transition temperature, and endothermic response are affected by prior thermal history[4,8,9] and by molecular weight.[1,2,10,11] Effects of molecular weight on the melt and/or cold crystallization kinetics of PPS have been studied.[1−16] The crystallization rate of PPS decreases as the molecular weight increases.[10,12] As a function of crystallization temperature, asymmetric linear growth rate curves are observed for PPS.[15,17]

The first purpose of the present work is to examine the effects of molecular weight on the structure of the amorphous phase in semicrystalline PPS. In this polymer, the amorphous phase has been shown to be highly constrained by the crystals, leading to a reduction in its molecular mobility.[4,8,9] The quantification of the effect of chain constraint was done initially through thermal analysis of the heat capacity increment, $C_p(T)$, at the glass transition.[4,89] Wunderlich's group found that the heat capacity increment at T_g was decreased by an amount much greater than that which could be anticipated on the basis of the known degree of crystallinity.[4] Subsequent dielectric relaxation experiments[9] also showed the signature of the constraining effects of the crystals on the amorphous phase mobility. Although many reports exists on the effects of molecular weight on crystallization kinetics,[1,2,10−16] until our work there had been no studies of the effects of molecular weight on the structure of the amorphous phase and the constraining effects of crystals. It was our hypothesis that lower molecular weight material would be more constrained by the crystals than higher molecular weight material. We imagine a picture in which the crystal/amorphous interphase would contain loops whose size and flexibility depend upon molecular weight. And, for a given length of amorphous phase "interlayer" between adjacent crystals, the shorter chains would be more likely to form interlamellar taut tie molecules that could contribute to reduced molecular mobility in the amorphous phase. Indeed, in a brief report of the results of temperature-modulated differential scanning

* To whom all correspondence should be addressed.
[†] Present address: Johnson and Johnson Research Center, Somerville, NJ 08876.
[⊗] Abstract published in *Advance ACS Abstracts,* September 15, 1997.

S0024-9297(96)01600-2 CCC: $14.00

Table 1. Intrinsic Viscosity and Viscosity Average Molecular Weight for the Fortron PPS Used in This Study

fortron PPS	intrinsic viscosity,[a] $[\eta]$ (g/dL)	viscosity av mol wt[b] M_v
F-200	0.20	30 000
F-214	0.29	50 000
F-300	0.45	91 000

[a] Intrinsic viscosities were measured in 1-chloronaphthalene at 208 °C. [b] M_v calculated using $M_v = (1.122 \times 10^4 [\eta])^{1.339}$.

calorimetry,[18] we found that lower molecular weight PPS was more constrained.

A second purpose of this work was to explore a range of crystallization temperatures that has so far been ignored in the study of amorphous phase structure. All prior work in this area, both in PPS[4,89] and in other high-performance polymers like PEEK,[19−21] has investigated the range of cold crystallization temperatures above the temperature, T', of fastest linear growth rate. This type of crystallization may be better termed "cold annealing" because of the inherent difficulty in heating the sample through T′ without initiating crystallization prior to equilibration at T_c. For PPS of medium molecular weight, T' is close to 150 °C. Cheng et al.[4] studied the constrained amorphous phase of PPS for $T_c = 170$°C and above. Our group studied cold crystallization temperatures of 150°C and above.[8,9] The present work is aimed at the cold crystallization temperature range above T_g but below T'. In this temperature range, crystallization kinetics become faster (crystallization half-time, $t_{1/2}$, decreases) as T_c increases.

Molecular weight is known strongly to affect the crystallization kinetics so that samples isothermally crystallizing at identical temperatures have done so at vastly different rates. Since the rate of formation of crystals will likely be an important factor in creating constraints on the amorphous phase, we decided to minimize this effect among the different molecular weight samples so that the influence of molecular weight on structure could more easily be assessed.

We characterize the relative phase fractions in our PPS materials using modulated differential scanning calorimetry (MDSC), normal DSC, and wide angle X-ray scattering (WAXS). Long periodicity, lamellar thickness, and crystallinity of lamellar stacks are evaluated in situ during isothermal crystallization using real-time small angle X-ray scattering. Finally, we investigate the effect of molecular weight on the mechanical properties of PPS using a combination of dynamic mechanical analysis (DMA) and MDSC.

2. Experimental Section

Three different molecular weight powders of Fortron PPS, from Hoechst Celanese, have been used in this investigation and are referred to as F-200, F-214, and F-300. All materials had a linear chain architecture. Intrinsic viscosity and viscosity average molecular weight (M_v) are summarized in Table 1. These PPS powders were dried inside a desiccator for several days at room temperature. Amorphous films were prepared by melting the powder in a hydraulic hot press between two pieces of Kapton film at 320°C for 2 min to destroy the crystallization seeds, followed by quenching into ice water. The amorphous samples obtained were transparent and showed no birefringence under crossed polarizers. Some of these amorphous samples were used directly in our study. Others were crystallized at different cold crystallization temperatures T_c until the completion of the crystallization.

A differential scanning calorimeter, DSC, Perkin-Elmer DSC-7, was utilized to study the isothermal crystallization kinetics of all the powders. The sample was encapsulated in an Al pan, loaded into the DSC cell at 60°C, and then heated at 20°C/min to T_c. The exothermic heat flow was monitored until the completion of the crystallization, at which time no further heat flow could be detected. A Perkin-Elmer DSC-4 was used to study the heat capacity increment at the glass transition, crystallization, and melting behavior of PPS. Indium was used to calibrate temperature and heat flow throughout the DSC study. The sample weight was around 8 mg, and a scan rate of 20°C/min was used. The heat of fusion of perfect PPS crystals was taken to be 112 J/g.[8]

A modulated DSC from TA Instruments was used to examine the initial degree of crystallinity and the ability for reorganization/recrystallization of PPS. A modulation amplitude of 0.318°C and a modulation period of 60 s were used to ensure that no cooling occurred during the experiments. The average sample weight was 8 mg, the heating rate was 2°C/min, and experiments were performed under a He flow of 30 mL/min.

SAXS experiments were performed at Brookhaven National Synchrotron Light Source using a high-intensity X-radiation source in transmission mode. The wavelength was 0.148 nm, and the sample-to-detector distance was about 1.46 m, calibrated using cholesterol myristate. The beam profile at the detector is 300 μm × 300 μm and can be treated according to a pinhole geometry. The isotropic SAXS intensity was circularly integrated and normalized for changes in incident beam intensity and sample absorption. A discrete Fourier transform[22] has been applied to the Lorentz-corrected intensity to obtain $K(z)$, the one-dimensional electron density correlation function, from

$$K(z) = \sum_{j=1}^{N} 4\pi I_{corr} s^2 \omega_N^{(j-1)(z-1)} \quad (1)$$

where

$$\omega_N = e^{-2\pi i/N} \quad (2)$$

In eq 1, z is the direction normal to lamellar stacks, N is the number of actual data points, I_{corr} is the intensity corrected for background and thermal density fluctuations, and s is the scattering vector ($s = 2 \sin \theta/\lambda$). Linear extrapolation of intensity from the beam stop region to $s = 0$ was used in the summation, while Porod's law[23] was applied to the high-s region. The resulting correlation function starts off with a z spacing of $1/s_{max}$, but a spline interpolation routine fills in the missing values in the region of interest. The treatment of Strobl and Schneider[24] was used for data analysis, yielding SAXS parameters of long period L and crystal thickness l_c. An estimate for the linear crystallinity, χ_{cl}, is made from either l_c/L or the correlation triangle (see ref 24 for details). A two-phase model is employed to obtain the amorphous interlayer thickness, l_a ($l_a = L - l_c$).

Dynamic mechanical analysis was carried out using a Seiko DMS 200 system under a nitrogen gas flow of 300 mL/min. The samples were cut into a 5 mm × 10 mm rectangular shape with a thickness of 0.6−1.0 mm. The scans were performed from 30 to ~240°C at a heating rate of 2°C/min, and data were collected at frequencies of 1, 2, 5, 10, and 20 Hz.

3. Results

3.1. Crystallization Kinetics. Cold crystallization kinetics of different molecular weight PPS samples were characterized using the Avrami equation.[25,26] The purpose of this analysis was to obtain the crystallization half-time, $t_{1/2}$, at which relative crystallinity = 0.5.

In Figure 1A, a generalized sketch of $t_{1/2}$ vs crystallization temperature is shown for two samples obeying different kinetics. The sample represented by curve A has a shorter half-life at any crystallization temperature than that shown by curve B. The minimum half-time for curve A occurs at the temperature marked as T'. The

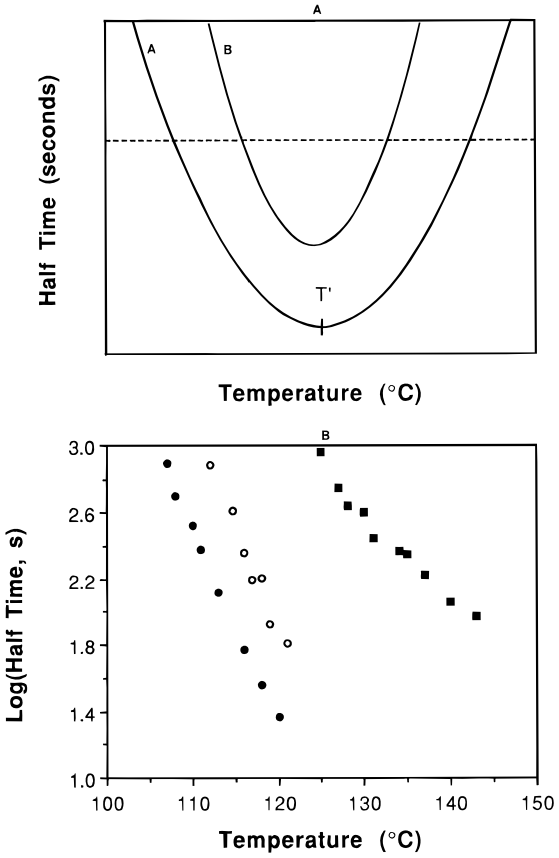

Figure 1. (A) Sketch of crystallization half-time, $t_{1/2}$, vs crystallization temperature for two materials exhibiting different kinetics. The dashed line represents a slice through the two curves at the same half-time. (B) Half-time, $t_{1/2}$ vs crystallization temperature for Fortron PPS from isothermal DSC: (●) F-200; (○) F-214; (■) F-300.

Table 2. Cold Crystallization Temperatures (±0.5 °C) Selected for Fortron PPS To Provide a Crystallization Half-Time of 200 or 700 s

half-time, s	F-200	F-214	F-300
200	110.6	116.0	135.0
700	107.0	112.0	125.0

horizontal dashed line represents a cut through both crystallization curves at the same half-time.

In Figure 1B, we plot $t_{1/2}$ vs temperature for the three different molecular weight samples studied here. We observe an increase in $t_{1/2}$ with increasing molecular weight, which indicates slower crystallization kinetics for the higher molecular weight sample consistent with other reports on PPS.[10−15] It is apparent from Figure 1B that isothermal crystallization studies in which T_c is held the same for all molecular weights would result in vastly different kinetics of crystallization among the samples. Comparisons of the effects of molecular weight on structure would suffer from the complications of crystallization rate differences. It is our intention to minimize the effects of the differences in kinetics of these different molecular weight PPS samples by crystallizing at temperatures giving all the samples the *same* half-time.

Through the curves in Figure 1B, we take a horizontal slice (as shown in Figure 1A) at half-times of 200 and 700 s and determine the cold crystallization temperature at the intersection point. These crystallization temperatures are listed in Table 2 for each molecular weight sample. From Table 2 we see that (approximately) a 4 deg change in T_c results in a change in half-time from 200 to 700 s for F-200 and F-214. A 10 deg change in T_c is required to change the half-time of F-300 by the same amount.

Table 3. Mass Fractions of Crystal, χ_c, Liquidlike Amorphous, χ_a, and Rigid Amorphous Phases, χ_{ra}, and Mass Fraction Linear Stack Crystallinity, $\chi_{1c}{}^m$, in Cold-Crystallized Fortron PPS after Crystallizing To Give a Half-Time of 200 or 700 s

Fortron PPS	$\chi_c{}^a$ (±0.02)	$\chi_a{}^b$ (±0.02)	$\chi_{ra}{}^c$ (±0.04)	$\chi_{1c}{}^{m\ d}$
	Half-Time = 200 s			
F-200	0.27	0.19	0.54	0.36
F-214	0.28	0.23	0.49	0.34
F-300	0.28	0.29	0.43	0.33
	Half-Time = 700 s			
F-200	0.26	*e*	*e*	0.36
F-214	0.25	0.20	0.55	0.34
F-300	0.26	0.24	0.50	0.34

[a] Determined from WAXS taken at room temperature. [b] Determined from DSC using eq 3. [c] Determined from eq 5. [d] Converted from SAXS linear crystallinity to mass fraction by density correction. Data taken at high temperature, at the completion of crystallization. [e] Value unable to be determined from DSC.

3.2. Thermal Properties. The mass fractions of the constituent phases were determined from WAXS and thermal analysis of well-crystallized samples using normal DSC scanning. Samples were crystallized inside a hot stage for a time equal to 6 times $t_{1/2}$, and then air-quenched to room temperature. The WAXS intensity of the semicrystalline material was used to determine the mass fraction crystallinity, χ_c, by subtraction of the scaled amorphous halo obtained from the WAXS pattern of purely amorphous samples. These results are almost exactly the same as the degree of crystallinity calculated from thermal analysis.[18] Crystallinity values are listed in the second column of Table 3. There is very little difference among the three molecular weight PPS samples crystallized under conditions giving the same $t_{1/2}$. When the half-time is increased (i.e., T_c is decreased) there is a small reduction in the degree of crystallinity for a given molecular weight. All the PPS samples have χ_c of 0.25−0.28 from WAXS.

Normal DSC at 20°C/min was used to determine χ_a, the amount of liquidlike amorphous phase contributing to the heat capacity step at T_g, $C_p(T)$, according to the following expression:[4,8,9]

$$\chi_a = C_p{}^{sc}(T)/C_p{}^{a}(T)|_{T=T_g} \qquad (3)$$

where the superscripts sc and a refer to the semicrystalline sample and the completely amorphous sample, respectively. Results are listed in the third column of Table 3. For material of the same molecular weight, higher χ_a is observed for the same crystallized with a faster crystalline rate, i.e., at a higher T_c. For PPS crystallized with the same $t_{1/2}$, the higher molecular weight sample contains a larger χ_a. That is, a larger amount of liquidlike amorphous phase contributes to the glass transition heat capacity increment in the higher molecular weight sample. These results agree with our previous MDSC study of these materials.[18]

3.3. Isothermal Crystallization Study Using SAXS. In Figure 2 we present the SAXS parameters for all three samples, grouped according to the two different half-times. The SAXS parameters vs time are shown for samples charactrized by $t_{1/2}$ = 200 s in Figure 2. Long period (Figure 2, lower curves marked A), shorter layer thickness (which we identify with the lamellar thickness) (Figure 2, middle curves marked B),

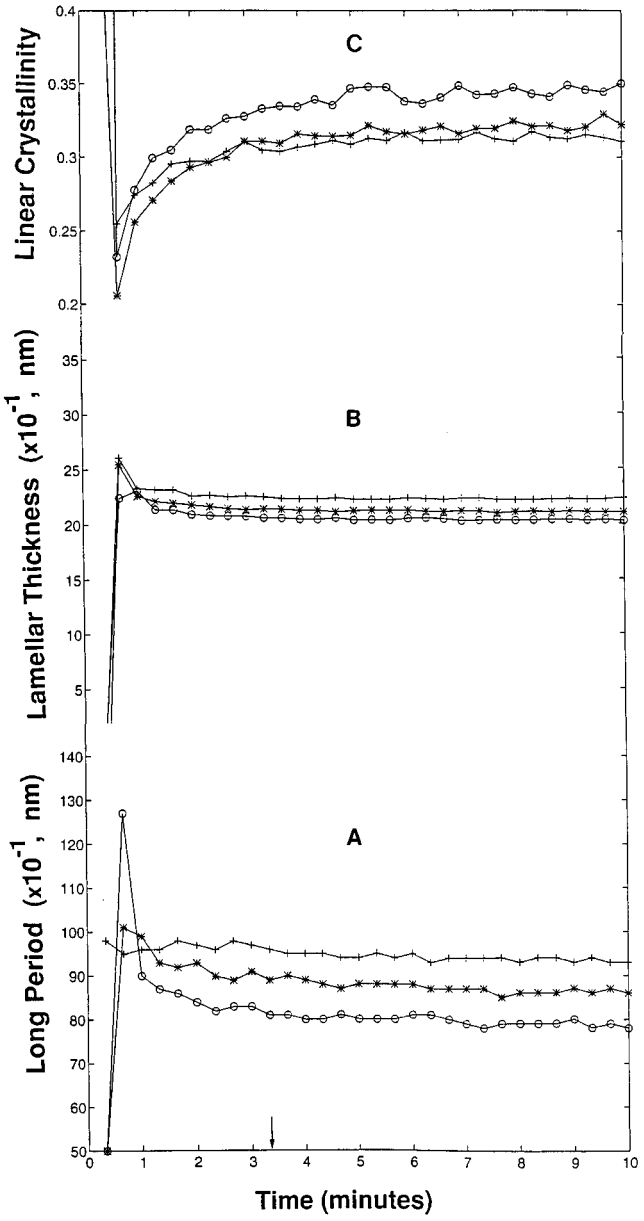

Figure 2. SAXS parameters as a function of crystallization time during isothermal cold crystallization of Fortron PPS with $t_{1/2} = 200$ s: (lower curves, A) long period, L; (Middle curves, B), lamellar thickness l_c; (upper curves, C) linear crystallinity, χ_c. Key: (○) F-200; (*) F-214; (+) F-300. Arrows indicate $t_{1/2}$.

and linear crystallinity (Figure 2, upper curves marked C) are plotted as functions of isothermal crystallization time. In these figures, the linear crystallinity was calculated from the correlation triangle.[24] Justification for the assignment of the shorter layer thickness to the lamellar thickness will be dealt with in the Discussion.

The arrow on the time axis indicates the crystallization half-time, $t_{1/2}$. We observe from Figure 2, that the lamellar structure develops very quickly for linear PPS. At very early times (represented by about the first two or three data points), the structure has not developed sufficiently to provide the density contrast for data analysis. Here, the SAXS parameters show erratic behavior. After this initial period, by a time about one-third of $t_{1/2}$, all parameters settle down, and the data now show only a little noise. The shapes of the curves indicate that the isothermal crystallization proceeds with the same kinetics for all three molecular weights, confirming our choice of the crystallization temperatures

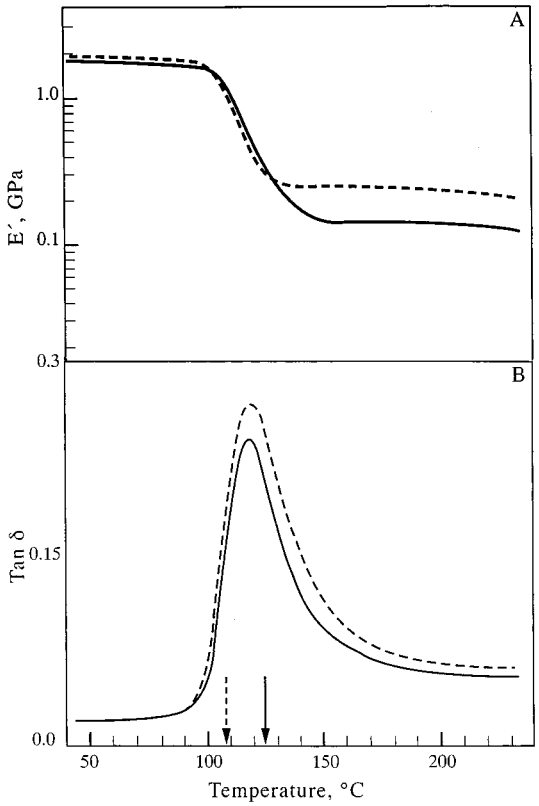

Figure 3. (Upper curves, A) modulus E' and (lower curves, B) tan δ, vs temperature for Fortron PPS F-300 (solid line) and F-200 (broken line) crystallized with $t_{1/2} = 700$ s, measured at 1 Hz. Arrows indicate T_c.

in Table 2. We observe at the end point of the crystallization that L is largest for the highest molecular weight. And, for the same material crystallized at different $t_{1/2}$, slightly larger L is observed for lower $t_{1/2}$ (higher T_c). A similar trend is observed in the lamellar thicknesses, except that within experimental errors, the differences in lamellar thickness are minimal. The trends in long period, lamellar thickness and linear crystallinity were the same for samples characterized by $t_{1/2} = 700$ s, and these data are not shown for the sake of brevity.

3.4. Dynamic Mechanical Properties. In order to explore the correlation between molecular weight and the mechanical properties of these cold-crystallized samples, we have performed DMA experiments on both the highest weight sample F-300 and the lowest molecular weight sample F-200. In Figure 3, we present the DMA data of F-300 and F-200 at 1 Hz, for materials crystallized with $t_{1/2} = 700$ s. We observed no appreciable changes in mechanical properties for F-300 and F-200 crystallized at other cold crystallization temperatures. Curves A and B represent the modulus E' and loss factor tan δ, respectively, changing as a function of temperature. F-300 data are indicated by the solid line, and F-200 by the broken line. The arrows indicate the cold crystallization temperature T_c. In the lower temperature region, we observe in Figure 3, curves A, that the modulus for F-300 (solid line) shows a glassy modulus of 1.8 GPa. As the temperature reaches 100°C, F-300 material starts to soften, resulting in a drop in E'. E' continues to drop about 1 order of magnitude and then flattens at 140°C with E' around 0.13 GPa. F-200 (broken line) has a slightly higher glassy modulus, before 100°C, then drops off as the temperature increases, and reaches a rubbery plateau

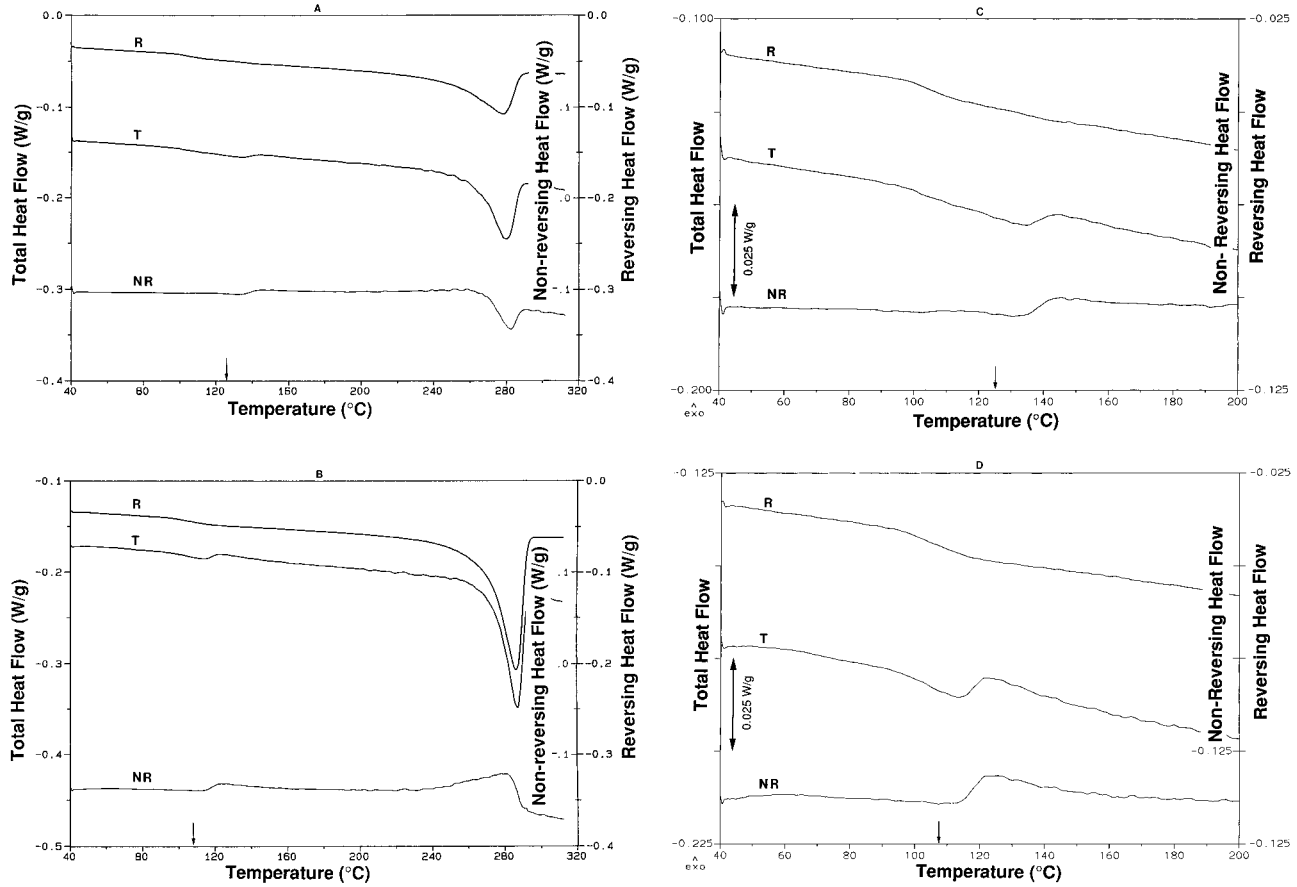

Figure 4. Total heat flow (T), reversing heat flow (R), and nonreversing heat flow (NR) from MDSC for Fortron PPS samples cold crystallized with a half-time of 700 s. Scan through the melting region: (A) F-300; (B) F-200. Expanded scale near the glass transition: (C) F-300; (D) F-200. Arrows indicate T_c.

after the temperature is above 130°C. F-200 has a much higher rubbery plateau modulus of 0.23 GPa.

In Figure 3, curves B, a strong asymmetric relaxation tan δ loss peak is observed for both F-300 (solid line) and F-200 (broken line). The peak maximum temperature for F-300 is around 120°C, and the peak height is about 0.24. The relaxation peak tan δ for F-200 has a peak maximum temperature of 120°C, with peak height about 0.26.

3.5. Modulated DSC Study. In order to understand what aspects of amorphous phase structure determine the mechanical properties of F-200 and F-300 at temperatures above T_c, we have used temperature-modulated DSC, or MDSC.[27,28] MSDC is able to separate the total heat flow (T) into two parts: one is the result of the heat capacity effect, such as glass transition and melting, often referred to as reversing heat flow (R); the other is the result of the non heat capacity effect, such as cold crystallization, often referred to as nonreversing heat flow (NR).[27−32] In this study, the same heating rate is used as in the DMA experiments to facilitate direct comparison. The three heat flow curves are plotted in Figure 4 for F-300 (4,A,C) and F-200 (4B,D), respectively. Parts C and D of Figure 4 reflect expanded views of the glass transition region. The arrows again indicate the temperatures at which the samples have been cold crystallized.

Figure 4A,C shows the MDSC results for the F-300 sample. In the total heat flow curve (T), a small step occurs at about 105°C as the result of the glass transition, followed by a small melting peak just above T_c (T_c = 125°C). Then an immediate upturn crystallization occurs at about 10 deg higher than T_c, followed by the major melting peak at about 278°C. These results are indentical to what we observed after normal DSC testing. In the reversing heat flow curve (R), the glass transition appears at 105°C, followed by a major melting peak at around 276°C. In the nonreversing heat flow curve (NR), the cold crystallization starts about 10 deg higher than T_c. The material continues to crystallize until the temperature reaches 270°C, and then a nonreversible melting occurs, driving the curve downward. All three curves become flat when the temperature is above 285°C, indicating that all the crystals have melted.

MDSC results of the F-200 sample with $t_{1/2}$ = 700 s are shown in Figure 4B,D. In the total heat flow curve (T), we observe that the glass transition and the small melting occur at the same time since T_c (T_c = 107°C) is very close to T_g. Following that, crystallization occurs, as the curve shows an upturn. A melting peak finally appears at about 287°C. In the reversing heat flow curve (R), a glass transition appears at about 110°C followed by a major melting peak with the peak maximum at 285°C. In the nonreversing heat flow curve (NR), a cold crystallization exotherm appears at about 10 deg higher than T_c. The F-200 material continues to crystallize as the temperature increases. The major exothermic peak appears at about 282°C. No melting endotherm is observed in the NR curve.

4. Discussion

4.1. Structure from SAXS. In analyzing the SAXS data presented in Figure 2, we adopt a simplified two-phase model in which the crystal lamellae alternate

with noncrystalline material of lower density. The long period, L, reflects the separation distance between the midpoints of two adjacent lamellae. The thicknesses of phase 1 (l_1) and phase 2 (l_2) are such that $l_1 + l_2 = L$, and $l_1 \leq l_2$. The thickness of phase 1 and the linear fraction of phase 1 (v_1) are estimated from the correlation triangle using the method of Strobl and Schneider.[24] SAXS data alone do not allow the distinction to be made in associating either phase 1 and phase 2 with the crystal lamellae (thickness l_c). Recently, two different approaches have been followed in the assignment of the crystal thickness. Jonas *et al*. chose the shorter length for l_c in their SAXS studies of PEEK[33] and PET[34] polymers. Fougnies *et al*.[35,36] for the PEEK polymer also chose l_c to be the shorter length, based upon the temperature evolution of the longer and shorter lengths. Only the shorter length increased with annealing temperature. The opposite choice was made by Hsiao *et al*.[37,38] for the PEEK polymer. In this work on PPS, we are in agreement with the assignments made by Jonas *et al*.[33,34] and Fougnies *et al*.[35,36] and assign the minority fraction (shorter length, l_1) to the crystal lamellae.

Jonas *et al*.[33] conclude that for PEEK $l_c < l_a$ since the density of the amorphous phase within the semicrystalline sample, ρ_{ac}, is greater than the density of the amorphous phase in the purely amorphous sample ρ_{a0}. The opposite choice, of longer length for l_c, would have resulted in a lower amorphous phase density, $\rho_{ac} < \rho_{a0}$, which is not observed experimentally. From our earlier work,[8] we showed that also in PPS $\rho_{ac} < \rho_{a0}$ for samples crystallized from the glassy state. Thus, the assignment of $l_c < l_a$ is consistent for PPS as for PEEK and PET.

The fraction of the crystal phase within the lamellar stacks, or the linear crystallinity, χ_{cl}, is related to the overall volume fraction crystallinity, Φ_c, according to

$$\Phi_c = \chi_s \chi_{cl} \tag{4}$$

where χ_s is the fraction of space filled by coherently scattering stacks of lamellae. Jonas *et al*.[33,34] reject $l_c > l_a$ because of implications for χ_s. $l_c > l_a$ results in χ_s values that are deemed unreasonably low for PEEK.[34] For PPS, the choice $l_c > l_a$ also would result in very low filling fractions, with χ_s ranging from 0.35 to 0.38. This would imply that very large amounts of amorphous phase material reside outside the lamellar stacks, which seems contrary to the observed dense space-filling nature of PPS spherulites.[5,39−42] In this work, therefore, we choose the minority component, v_1, as the crystal phase. Then the shorter length l_1 represents the lamellar thickness and v_1 is the linear crystallinity of the lamellar stacks, as plotted as Figure 2.

In prior work we used SAXS to study the structure of Ryton PPS[8] after isothermal melt or cold crystallization. In that work we used simple application of Bragg's law to determine the long period, and l_c was found by multiplying L by the bulk crystallinity. For cold crystallization, the long period weakly decreased as T_c decreased, and at the lowest T_c investigated (150°C), $L \sim 102$ Å.[8] We also found that l_c decreased as T_c decreased, and at $T_c = 150$°C, l_c was 29 Å,[8] which is very comparable to the values of l_c determined here for Fortron PPS.

Figure 2B indicates that the lamellae develop their ultimate thickness, l_c, early in the crystallization process. For both crystallization conditions and all three molecular weights, l_c reaches a constant value at times shorter than the crystallization half-time (at $t \sim 0.5t_{1/2}$). On the other hand, the long period (Figure 2A) continues its overall decreasing trend until the half-time has been exceeded (at $t \sim 1.5t_{1/2}$). The result that L decreases and l_c remains constant is in agreement with the observations of Jonas *et al*. for PEEK *nonisothermally* crystallized from the quenched amorphous state.[33]

During the time that L decreases while l_c is constant, we conclude that the average amorphous layer thickness, l_a, decreases. We suggest that as the spherulites grow isothermally, the lamellar thickness is controlled predominantly by the crystallization temperature, through the degree of undercooling. But the average long period decreases during crystallization, even after spherulite impingement at $\sim t_{1/2}$, because the crystals are forced to grow into smaller available spaces among surrounding crystals. These space constraints, rather than being asserted on the crystal thickness, are felt within the amorphous phase, causing reduced l_a.

In Table 3, we compare the linear crystallinity with the crystallinity determined from room temperature WAXS analysis. Caution must be used in interpretation of the WAXS estimates, especially in systems crystallized at very low temperatures where imperfect crystals and other rigid, but noncrystalline objects may be formed. We found a very close agreement[18] between the crystallinity determined by WAXS and that from DSC. Since noncrystalline entities are unable to contribute to melting endotherms, we believe that this justifies our use of the WAXS crystallinity in the present work. In comparison to the room temperature WAXS data, the SAXS linear crystallinity is taken at the end point of the crystallization and is a high-temperature measurement. The bulk crystallinity from WAXS is systematically lower than the linear stack crystallinity, χ_{cl}, obtained from the SAXS correlation triangle.[24] This indicates some portion of the amorphous phase resides outside the lamellar stacks, resulting in higher linear crystallinity within the lamellar stacks.

From Table 3, we see that higher molecular weight material has a slightly smaller χ_{cl} compared with lower molecular weight material. We conclude that there is slightly more amorphous phase within the lamellar stacks in the higher molecular weight sample. However, the experimental errors on the χ_{cl} measurement are large.

4.2. Thermal Analysis. Thermal analysis at 20°C/min was used to determine χ_{ra}, the fraction of amorphous chains constrained by the crystals (and *not* contributing to the heat capacity increment), from

$$\chi_{ra} = 1 - \chi_c - \chi_a \tag{5}$$

The rigid amorphous fractions are listed in the fourth column of Table 3. Since the degree of crystallinity is virtually the same, this implies that there is a larger rigid amorphous fraction in samples with lower molecular weight. In F-200, $\chi_{ra} = 0.54$, while in F-300 $\chi_{ra} = 0.43$. While the error bars are larger on the χ_{ra} measurement, we note that this trend in χ_{ra} has been followed consistently through two sets of samples crystallized independently, and five different experiments in which either DSC or MDSC[18] was used to analyze the χ_{ra} content.

For the same molecular weight material, the sample is more highly constrained when crystallized at a slower crystallization rate, i.e., at lower temperature. For example, in Table 3 we see that F-300 has $\chi_{ra} = 0.43$ for $t_{1/2} = 200$ s, and this increases to $\chi_{ra} = 0.50$ when $t_{1/2}$ increases to 700 s. In our previous cold crystallization study on Ryton PPS,[9] χ_{ra} decreased from 0.42 to

Table 4. Heat of Fusion, ΔH, of Cold-Crystallized Fortron PPS Determined from Modulated Differential Scanning Calorimetry Curves of Total Heat Flow, T, Reversing Heat Flow, R, and Nonreversing Heat Flow, NR

Fortron PPS[a]	ΔH^T, J/g (±0.5)	ΔH^R, J/g (±0.5)	ΔH^{NR}, J/g (±0.5)
F-200	27.3	81.5	−52.2
F-300	28.9	42.7	−14.8

[a] Crystallized at a temperature giving a half-time of 700 s.

0.33 when T_c increased from 150 to 210°C. Thus, current results on Fortron PPS agree well with our previous study on Ryton PPS (Phillips Petroleum) and suggest that crystals cause a very highly constrained amorphous phase interlayer when T_c gets close to T_g.

The location of the rigid amorphous phase is suggested to be between lamellar crystals, possibly near the crystal/amorphous interphase.[4] We propose that the lower molecular weight PPS has a greater number of taut tie molecules between the crystals, resulting in a larger fraction of constrained amorphous phase. The higher molecular weight PPS still has more entanglements within the amorphous phase and therefore has a slightly higher glass transition temperature and slower crystallization kinetics. But once crystals form at low temperatures close to T_g, the longer molecular length chains do not appear to become as constrained as do the shorter chains.

4.3. Mechanical Properties. It is generally considered that higher molecular weight material has better mechanical properties because of higher density of chain entanglements.[43−45] Obvservation of a lower E' for F-300 at the higher temperature was unexpected. However, in the high-temperature region, the temperature increases above the cold crystallization temperature T_c (represented by the arrows shown in Figure 3). When the temperature rises above the crystallization temperature, we expect there to be changes in polymer structure, for example, perfecting of existing crystals or formation of new crystals. We postulate that these structural changes for $T > T_c$ result in the lower E' observed in the higher molecular weight F-300.

These changes were observed in the MDSC scans of F-200 and F-300 shown in Figure 4. The heats of fusion from the three heat flow curves are calculated, and the results are shown in Table 4. Comparing Figure 4A,B, three significant differences in the thermal behavior between F-300 and F-200 can be seen. First, the melting temperatures of the major peaks in both the T and R curves of the F-200 sample are higher than those of the F-300 sample. Second, in the nonreversing heat flow curve (NR), F-300 shows both exothermic behavior and nonreversing melting at the higher temperature, while F-200 gives only an exothermic peak. Third, we observe that even though the two materials have initially about the same crystallinity (same area under the total heat flow curve in Table 4), the relative areas under the reversing and nonreversing heat flow curves are quite different.

Analysis of MDSC scans in the melting region is still a subject of intense debate.[29,46] Nonetheless, we may compare the *relative* behavior of these materials treated with the same MDSC protocol. Although instrumental thermal lag may change the apperance of the reversing and nonreversing heat flow curves, we expect these effects to be similar for samples of similar mass. Therefore, the changes seen in the reversing and nonreversing heat flow curves may tentatively be identified with real behavior of the materials, reflecting differences in ability for reorganization during MDSC scanning. It appears that F-200 has a greater ability to reorganize and form more crystals during the heating scan than F-300. Since the DMA experiments stop at an earlier stage, we have also examined the amount of crystals formed in these materials before 240°C and find that relatively more crystals formed in F-200 than in F-300 by this temperature.

DMA and MDSC results can be compared directly since they are performed using the same heating rate. The three major differences between F-300 and F-200 from MDSC suggest that F-200 and F-300 have different crystallizabilities. F-300 has a higher molecular weight, and its crystallization is slowed by the large amount of chain entanglement. Consequently, it has a slower reorganization/recrystallization rate. Therefore, in F-300 material we observe a smaller amount of exothermic heat flow during the heating scan and a lower T_m. In contrast, F-200 is a lower molecular weight material and tends to crystallize very fast. It also has the ability to reorganize fast. Therefore, we observe more crystals forming during the scan and a higher T_m. Generally speaking, the infinite crystal melting temperature (T_m^0) increases as the molecular weight increases, since it corresponds to the largest extended chain crystals possibly formed by the material. However, polymer crystallization is controlled by kinetics, rather than thermodynamics. Therefore, as the temperature increases, lower molecular weight PPS has better reorganization ability and continues to form metastable crystal lamellae that melt at a higher temperature. We believe the differences in crystallizability and reorganization ability between F-200 and F-300 also account for the difference in E' observed at higher temperature. In both F-200 and F-300 samples, E' was unaffected by the crystallization temperature. Since lower molecular weight material tends to crystallize faster and form more crystals, the amorphous polymer chains may be under constant and large constraints by the formed crystals. In contrast, the higher molecular weight material requires a longer time to crystallize and reorganize, and therefore fewer constraints are asserted by the crystals. This idea is supported by the smaller amount of constrained amorphous phase formed in F-300. Thus, at higher temperature, we observe a lower E' for F-300 and a higher E' for F-200.

5. Conclusions

The effect of molecular weight on the cold crystallization behavior and mechanical properties of linear PPS Fortron has been investigated. We observe the existence of large rigid amorphous fractions in the cold-crystallized sample in agreement with our previous studies,[8,18] and the lower the T_c, the higher the χ_{ra}. The same crystallinities are found in these cold-crystallized samples. For different molecular weight samples crystallized with the same $t_{1/2}$, the more mobile amorphous phase is observed in the higher molecular weight material, which leaves it with a less rigid amorphous phase.

The effects of both molecular weight and T_c on the mechanical properties of PPS have been investigated by combining DMA and MDSC. It is found in DMA that molecular weight is the determining factor that affects the E' value at the higher temperature, since the same modulus E' and loss factor tan δ are observed for the samples crystallized at different T_c. A lower E' is

observed for the higher molecular weight material. MDSC data suggest that higher molecular weight PPS has a slower crystallization rate and reorganization rate. The amount of crystals formed during heating is smaller in high molecular weight PPS, and this may be the explanation for the reduced Young's modulus above T_g.

Acknowledgment. Research was supported by the Army Research Office through contracts DAAH04-96-1-0009 and DAAH04-94-G-0317. The authors thank Hoechst Celanese for different molecular weight Fortron samples and Dr. George Collins for providing sample information. We also thank Dr. Leonard Thomas and Mr. David Geller from TA Instruments for providing the MDSC and for the discussions of MDSC experimental parameters.

References and Notes

(1) Chung, J. S.; Cebe, P. *Polymer* **1992**, *33*, 2312.
(2) Chung, J. S.; Cebe, P. *Polymer* **1992**, *33*, 2325.
(3) Brady, D. J. *J. Appl. Polym. Sci.* **1976**, *20*, 2541.
(4) Cheng, S. Z. D.; Wu, Z. Q.; Wunderlich, B. *Macromolecules* **1987**, *20*, 2802.
(5) Lopez, L. C.; Wilkes, G. L. *J. Macromol. Sci., Rev. Macromol. Chem. Phys.* **1989**, *C29*, 83.
(6) Geibel, J. F.; Campbell, R. W. In *Poly(phenylene sulfide)s*; In Comprehensive Polymer Science; Pergamon Press: Oxford, U.K., 1989; Vol. 5, p 543.
(7) Cebe, P. *Polym. Composites* **1995**, *3*, 239.
(8) Huo, P. P.; Cebe, P. *Colloid Polym. Sci.* **1992**, *270*, 840.
(9) Huo, P. P.; Cebe, P. *J. Polym. Sci., Polym. Phys. Ed.* **1992**, *30*, 239.
(10) Lopez, L. C.; Wilkes, G. L. *Polymer* **1988**, *29*, 106.
(11) Lopez, L. C.; Wilkes, G. L.; Geibel, J. F. *Polymer* **1989**, *30*, 147.
(12) Lovinger, A. J.; Davis, D. D.; Padden, F. J. *Polymer* **1985**, *26*, 1595.
(13) Menczel, J. D.; Collins, G. L. *Polym. Eng. Sci.* **1992**, *32*, 1264.
(14) Collins, G. L.; Menczel, J. D. *Polym. Eng. Sci.* **1992**, *32*, 1270.
(15) Chung, J. S.; Cebe, P. *J. Polym. Sci., Polym. Phys. Ed.* **1992**, *30*, 163.
(16) Budgell, D. R.; Day, M. *Polym. Eng. Sci.* **1991**, *31* (7), 1271.
(17) Hsiao, B. S.; Chang, I. Y.; Sauer, B. B. *Proc. 49*th *SPE ANTEC*, XXXVII, **1991**, 2084.
(18) Lu, S. X.; Cebe, P. *J. Thermal Anal.* **1997**, *49*, 525.
(19) Cheng, S.; Cao, M.; Wunderlich, B. *Macromolecules* **1986**, *19*, 1868.
(20) Huo, P. P.; Cebe, P. *Macromolecules* **1992**, *25*, 902.
(21) Sauer, B. B.; Hsiao, B. S. *Polym. Prepr. (Am. Chem. Soc., Div. Polym. Chem.)* **1995**, *36* (1), 261.
(22) *Matlab Reference Guide*; The Math Works, Inc.: Natick, MA, 1992, p 182.
(23) Porod, G. *Kolloid Z. Z. Polym.* **1951**, *124*, 83.
(24) Strobl, G. R.; Schneider, M. J. *J. Polym. Sci., Polym. Phys. Ed.* **1980**, *18*, 1343.
(25) Avrami, M. *J. Chem. Phys.* **1939**, *7*, 1103.
(26) Avrami, M. *J. Chem. Phys.* **1940**, *8*, 212.
(27) Reading, M.; Hahn, B. K.; Crowe, B. S. U.S. Patent 5,346,-306, 1994.
(28) Marcus, S. M.; Reading, M. U.S. Patent 5,335,993, 1994.
(29) International Congress on Thermal Analysis and Calorimetry. Modulated DSC Workshop, Philadelphia, PA, 1996.
(30) Wunderlich, B.; Jin, Y.; Boller, A. *Thermochim. Acta* **1993**, *238*, 277.
(31) Reading M. *Trends Polym. Sci.* **1994**, *8* (1), 248.
(32) Boller, A.; Jin, Y.; Wunderlich, B. *J. Thermal Anal.* **1994**, *42*, 307.
(33) Jonas, A. M.; Russell, T. P.; Yoon, D. Y. *Macromolecules* **1995**, *28*, 8491.
(34) Jonas, A. M.; Russell, T. P.; Yoon, D. Y. *Colloid Polym. Sci.* **1994**, *272*, 1344.
(35) Fougnies, C.; Damman, P.; Villers, D.; Dosiere, M.; Koch, M. H. J. *Macromolecules* **1997**, *30* (5), 1385.
(36) Fougnies, C.; Damman, P.; Dosiere, M.; Koch, M. *Macromolecules* **1997**, *30* (5), 1392.
(37) Hsiao, B. S.; Sauer, B. B. *J. Polym. Sci., Polym. Phys. Ed.* **1993**, *31*, 901.
(38) Hsiao, B. S.; Gardner, K. H.; Wu, D. A.; Chu, B. *Polymer* **1993**, *34*, 3996.
(39) Huo, P. P.; Chung, J. S.; Cebe, P. *Polym. Composites* **1992**, *13*, 346.
(40) Uemura, A.; Isoda, S.; Tsuji, M.; Ohara, M.; Kawaguchi, A.; Katayama, K. I. *Bull. Inst. Chem. Res. Kyoto Univ.* **1986**, *64*, 66.
(41) Bretas, R.; De Jesus, M.; Lunardi, G. *J. Mater. Sci.* **1992**, *27*, 2345.
(42) Waddon, A. J.; Hill, M. J.; Keller, A.; Blundell, D. J. *J. Mater. Sci.* **1987**, *22*, 1773.
(43) Flory, P. J. *Principles of Polymer Chemistry*; Cornell University Press: Ithaca, NY, 1990.
(44) Wunderlich, B. *Macromolecular Physics*; Academic Press: New York, 1976; Vol. 2.
(45) Ward, I. M. *Mechanical Properties of Polymers*; John Wiley & Sons: New York, 1974.
(46) Sichina, W. *Proc. NATAS Conf.*; *24*th **1995**, 123.

MA961600E